# Synchronizing outdoor heatwave detection with indoor thermal extremes: A case study in Brazilian social housing

**Matheus Körbes Bracht[1], Ana Paula Melo[1] and Roberto Lamberts[1]**

[1] LabEEE/UFSC, Florianópolis (Brazil)

### Abstract

With climate change intensifying the frequency and severity of heatwaves, understanding their impact on indoor environments is critical for occupant health and energy resilience. This study investigates the alignment between two heatwave detection methods (WMO/INMET and Ouzeau et al., 2016) and indoor key performance indicators of a simulated social housing unit located in Brasília, Brazil. Using EnergyPlus program and historical weather data (1991–2023), we assessed the overlap between the detection methods and three indoor indicators: maximum operative temperature, Heat Index, and total cooling load. Results show a low temporal overlap between outdoor detections and indoor extremes, varying across thermal zones and depending on the building envelope characteristics. The Ouzeau et al. (2016) method showed greater sensitivity and better agreement with operative temperature and Heat Index extremes. However, both methods failed to capture peak cooling load periods, likely due to the omission of humidity and solar gains in their criteria. These findings highlight the need to refine heatwave definitions for indoor stress assessment and energy planning, particularly for off-grid and battery-supported systems.

*Keywords: Heatwaves, extreme weather events, building simulation, thermal stress, peak loads.*

## 1. Introduction

Heatwaves have become more frequent, longer, and more intense due to anthropogenic climate change (IPCC, 2023). These events have severe impact on human health, with numerous studies linking extreme temperatures to elevated mortality and morbidity, particularly among vulnerable populations (Faurie et al., 2022). In addition to public health concerns, heat waves impose operational challenges on buildings and energy systems: thermal loads increase, cooling system efficiency declines, and high ambient temperatures reduce power generation capacity (Gautier et al., 2022).

There is currently no universally accepted definition of a heat wave based on measurable parameters, as perceptions of heat waves vary by local context (Roetzel et al., 2010). In scientific literature, diverse approaches are employed: some definitions are impact-oriented, focusing on excess mortality or discomfort, whereas others are meteorological, identifying statistical temperature anomalies over reference periods (Machard et al., 2020). Consequently, a variety of thresholds and parameters have been proposed to detect these events (Perkins & Alexander, 2014).

Despite the growing body of literature on heatwaves, relatively few studies examine their direct effects on the indoor environment. Building energy simulations (BES) show that indoor thermal conditions do not always align with outdoor metrics, as solar radiation, occupancy schedules, and envelope characteristics significantly shape internal responses (Guo et al., 2019).

Moreover, the most critical impacts of extreme events often arise from the co-occurrence of multiple stressors rather than from a single variable reaching an absolute extreme. For example, prolonged periods of high temperature combined with elevated humidity can exacerbate human thermal stress (Chen et al., 2019). Conversely, in energy systems, compound extremes may occur when high electricity demand coincides with reduced renewable generation, such as low wind or solar output, increasing grid vulnerability (Graczyk et al., 2024).

Assessing how heatwave detection methods perform under distinct climatic regimes is therefore essential. This is particularly true for tropical regions with alternating wet and dry seasons, where simultaneous thermal and humidity extremes can differ sharply between seasons. The central plateau of Brazil provides such a context, with Brasília serving as a representative case of the tropical savanna (Aw) climate.

Brasília experiences two distinct seasons: a rainy period from October to April and a dry period from May to September. Despite its relatively mild conditions due to its high altitude (1,060.4 m), long-term observations show a


10.18086/swc.2025.09.21 Available at http://proceedings.ises.org

steady increase in both mean and maximum temperatures since the city's foundation in the 1960s. These trends have significant implications for cooling energy demand and passive survivability in buildings (Bracht et al., 2023). The same study, which analyzed the 1961–2021 period, found that the critical year varies depending on the performance indicator and building envelope, reinforcing the importance of assessing climate-based extremes in this region.

Building upon this context, the study aims to evaluate how different heatwave detection methods reflect indoor thermal and energy performance. Simulations were conducted for a typical single-family social housing unit in Brasília, Brazil, considering two envelope types (high and low thermal inertia). The analysis investigates the synchronization between detected heatwaves and internal peak conditions considering three different key performance indicators (KPIs).

# 2. Method

To address these objectives, the method integrates climate data analysis and building energy simulations. Section 2.1 presents the climate dataset and the heatwave detection methods applied, Section 2.2 describes the building model, boundary conditions and simulation setup, and Section 2.3 details the synchronization calculation.

## 2.1 Climate data and detection methods

A historical climate dataset for Brasília, Brazil, was used to characterize local weather conditions. The series comprises hourly records (1991–2023) from Brasília Airport, complemented with ERA5 solar radiation data. Each year of the dataset was formatted according to the EnergyPlus Weather File (EPW) data dictionary (DOE, 2025) and used as the input weather file for the simulations. This dataset forms the basis of the Typical Meteorological Year (TMY) climate files available at the Climate.OneBuilding website (Crawley & Lawrie, 2025).

Two heatwave detection methods were applied considering this dataset:

1) WMO/INMET method: Used by Brazil's National Meteorological Institute (INMET) for issuing heat alerts, this method, based on the definition of the World Meteorological Organization (WMO), defines a heatwave as two or more consecutive days with daily maximum temperature ≥ 5 °C above the monthly average (INMET, 2025).

2) Ouzeau et al. (2016) method: Adopted in the IEA EBC Annex 80 project (IEA, 2025), this method identifies heatwaves based on daily mean temperature percentiles calculated over a 30-year baseline: *Spic* (99.5%) defines the extreme-event threshold, *Sdeb* (97.5%) marks the start and end, and *Sint* (95%) represents the interruption threshold. A heatwave starts when the daily mean temperature exceeds *Sdeb* and ends after three consecutive days below it, or immediately if it falls below *Sint*.

For both methods, the 1991-2020 period was used as the 30-year climatological baseline to define the necessary thresholds.

## 2.2 Building simulation

Based on the climate dataset described above, building energy simulations were performed using EnergyPlus (version 25.1). The simulations followed the guidelines of the Brazilian thermal performance standard (ABNT, 2024) and were conducted under two operating conditions: naturally ventilated and mechanically conditioned.

For the conditioned scenario, the air-conditioning system was modeled as an *Ideal Loads Air System* with a heating setpoint of 21 °C and a cooling setpoint of 24 °C. The outputs are hourly heating and cooling thermal loads. In the naturally ventilated scenario, the *AirFlowNetwork* system was used, considering a sliding window with a maximum opening factor of 0.45, controlled by indoor and outdoor temperatures. Windows were set to open if all the following requirements were met: (1) the space was occupied; (2) the indoor temperature exceeded 19 °C; and (3) the indoor temperature was higher than the outdoor temperature.

The occupancy schedule followed the operational profile defined in the Brazilian standard (ABNT, 2024). Bedrooms were assumed to be occupied from 22:00 to 08:00, and the living room from 15:00 to 22:00, reflecting typical household activity. Internal gains from occupants, lighting, and appliances were included according to the Brazilian thermal performance standard assumptions (Table 1).

**Table 1 Internal loads and schedules configuration according to NBR 15575 requirements.**

| Internal load | Living room | Bedrooms |
|---|---|---|
| **Number of people** | 4 people | 2 people |
| **Lighting** | 5 W/m² | 5 W/m² |
| **Equipment** | 120 W | 0 W |
| **Activity level** | 108 W | 81 W |
| **Occupation period** | 15:00 to 22:00 | 22:00 to 08:00 |

Key performance indicators (KPIs) included the maximum operative temperature (°C), Heat Index (°C) and total cooling load (W), used to assess synchronization with outdoor extremes and detected heatwaves. The Heat Index values were obtained directly from the EnergyPlus output variable “Zone Heat Index”, which estimates the apparent temperature perceived by occupants based on simulated air temperature and relative humidity within each thermal zone. This indicator was used to represent combined temperature-humidity effects on indoor thermal stress. This approach enables the evaluation of how well heatwave detection methods represent indoor overheating and cooling energy demand.

Figure 1 illustrates the reference geometry used in the EnergyPlus models. The reference model represents a typical social housing Brazilian single-family dwelling (Triana et al., 2015), with a total floor area of 43.24 m², two bedrooms (8.85 m² and 8.30 m²), a combined living room and kitchen (21.43 m²), one bathroom (4.66 m²), and a ceiling height of 2.50 m.


**Figure 1: Simulation model and floor plan of the reference case.**

To assess differences in thermal inertia and their influence on synchronization, two envelope variants were modeled:

- Case 1 (High Thermal Inertia): concrete walls and roof with fiber cement tiles over a concrete slab.
- Case 2 (Low Thermal Inertia): light steel frame (LSF) structure with insulation in both external walls and roof.

Table 2 presents the thermal properties of the building components of each case considered.

**Table 2: Thermal properties of the building components.**

| Building component | Thermal transmittance* (W/m²K) | | Thermal capacity (kJ/m²K) | | Solar absorptance (-) |
|---|---|---|---|---|---|
| | **Case 1** | **Case 2** | **Case 1** | **Case 2** | |
| Internal walls | 3.37 | 1.96 | 220 | 25 | - |
| External walls | 4.84 | 0.52 | 220 | 26 | 0.58 |

| Building component | Thermal transmittance* (W/m²K) | | Thermal capacity (kJ/m²K) | | Solar absorptance (-) |
|---|---|---|---|---|---|
| | Case 1 | Case 2 | Case 1 | Case 2 | |
| Roof | 2.42 | 0.36 | 220 | 34 | 0.65 |

*U-Factor with Film from EnergyPlus' outputs

The transparent elements have a solar heat gain coefficient of 0.87 and a thermal transmittance of 5.70 W/(m²·K). The *GroundDomain:Slab* object was employed to simulate ground contact, with the floor properties compliant with the NBR 15575 standard. These correspond to a 10 cm concrete slab featuring a thermal conductivity of 1.75 W/(m·K), a specific heat of 1000 J/(kg·K), a solar absorptance of 0.65, and a 2,200 kg/m³ density.

## 2.3 Synchronization calculation

To evaluate synchronization, heatwave periods detected by both methods in the historical series were first compared to determine their overlap rate. For each indoor KPI, the 99th percentile was calculated as the threshold for extreme values for each construction case (concrete and LSF) and each simulated room (Bedroom 1, Bedroom 2, and Living Room). The hours in which the KPI exceeded this threshold (99th percentile) were identified as indoor extreme events.

Synchronization was quantified as the fraction of indoor extreme hours that occurred simultaneously with outdoor heatwave periods. For each construction case *c* and room *r*, the set of extreme hours $E_{c,r}$ was defined as:

$$E_{c,r} = \{t : X_{c,r}(t) > \tau_{c,r} \; and \; \Omega_r(t) = 1\} \qquad \text{(eq. 1)}$$

where $X_{c,r}(t)$ is the hourly value of the indoor indicator (operative temperature, heat index, or cooling load), $\tau_{c,r}$ is its 99th percentile threshold, and $\Omega_r(t)$ represents the occupancy schedule of the corresponding room (1 for occupied hours, 0 otherwise).

Synchronization with each detection method $m$ (INMET or Ouzeau) was then computed as:

$$S_{c,r}^{(m)} = 100 \times \frac{\sum_{t \in E_{c,r}} H_m(t)}{|E_{c,r}|} \qquad \text{(eq. 2)}$$

where $H_m(t)$ is a binary variable equal to 1 during hours identified as heatwaves by method $m$. $S_{c,r}^{(m)}$ therefore expresses the percentage of extreme indoor hours coinciding with detected heatwave periods. The code developed for the heatwave detection and synchronization procedure is openly available in a GitHub repository (Bracht, 2025).

# 3. Results

As a first step, threshold values for each detection method were determined. Table 3 presents the monthly climatological normals and the corresponding thresholds (normal + 5 °C) of maximum daily temperature for the 1991–2020 historical series. These values were then used to identify heatwave events according to the WMO/INMET method. The highest thresholds occur in September and October, coinciding with the transition between the dry and rainy seasons.

**Table 3: Mean daily maximum temperature for each month and the threshold for heatwave detection according to WMO/INMET method.**

| Month | Jan | Fev | Mar | Apr | May | Jun | Jul | Aug | Sep | Oct | Nov | Dec |
|---|---|---|---|---|---|---|---|---|---|---|---|---|
| **Daily normal (°C)** | 27.8 | 28.1 | 27.8 | 27.8 | 27.0 | 26.3 | 26.4 | 28.2 | 29.8 | 29.7 | 27.7 | 27.6 |
| **Threshold (°C)** | 32.8 | 33.1 | 32.8 | 32.8 | 32.0 | 31.3 | 31.45 | 33.2 | 34.8 | 34.7 | 32.7 | 32.6 |

Table 4 presents the threshold values derived from the method proposed by Ouzeau et al. (2016) for the same historical period. Unlike the WMO/INMET approach, which uses maximum daily temperature, this method is based on daily mean temperature percentiles.

**Table 4: Percentile thresholds (Ouzeau et al., 2016) for Brasília (1991–2020).**

| Indicator | Sint (95th percentile) | Sdeb (97.5th percentile) | Spic (99.5th percentile) |
|---|---|---|---|
| Daily mean temperature (°C) | 25.28 | 25.92 | 27.10 |

Figure 2 shows the periods identified as heatwaves throughout the historical series, along with the annual number of hours classified as extreme events. It can be observed that the method by Ouzeau et al. detected a greater number of heatwave events, although detections only began from 1997 onwards. Moreover, this method consistently captured a higher number of extreme hours compared to the WMO/INMET method, except for the early years of the series and in 2015. A total of 984 hours were simultaneously identified as heatwave periods by both methods, representing 19.62% of all hours with any detection.

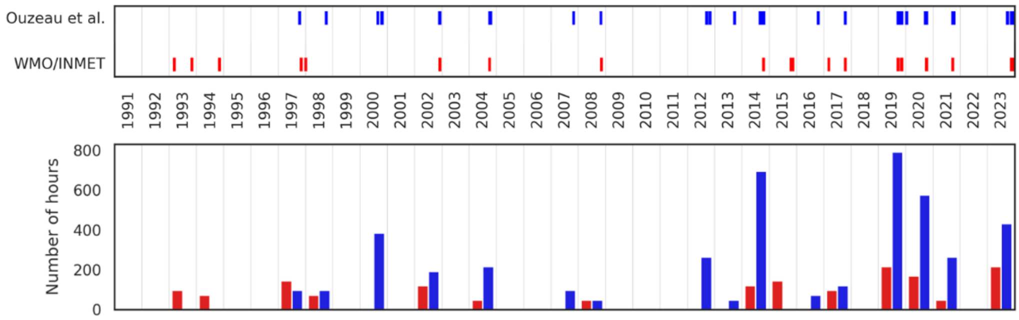


**Figure 2: Heatwave events during the historical period.**

A low overlap between the two methods was expected, since the WMO/INMET criteria can identify abnormally hot periods even during cooler months (as it is based on monthly normals), whereas the Ouzeau et al. (2016) method is more likely to detect events occurring during traditionally warm seasons, due to the use of fixed percentile thresholds over the entire historical series.

Based on the building energy simulation results, $99^{th}$-percentile thresholds were established for each indoor performance indicator (Table 5). It is worth noting that Case 1 (high thermal inertia) reached higher operative temperatures, Heat Index values and cooling rates than Case 2, as the greater thermal capacity did not compensate for the lower insulation of its envelope. Furthermore, the living room consistently exhibited higher values of operative temperature and cooling rate due to its predominant daytime occupancy, coinciding with higher outdoor temperatures and direct solar gains. These distinct threshold levels directly influence the subsequent synchronization analysis, since they determine the frequency and timing of hours classified as indoor extremes for each case and thermal zone.

**Table 5: Threshold values for each indicator, case and room based on BES.**

| Room | Operative Temp. (°C) | | Heat Index (°C) | | Cooling Rate (W/m²) | | Area (m²) |
|---|---|---|---|---|---|---|---|
| | Case 1 | Case 2 | Case 1 | Case 2 | Case 1 | Case 2 | |
| Bedroom 1 | 29.3 | 27.3 | 29.2 | 27.4 | 86.7 | 44.9 | 8.85 |
| Bedroom 2 | 29.4 | 27.4 | 29.3 | 27.5 | 92.8 | 53.7 | 8.30 |
| Living room | 34.0 | 33.4 | 34.1 | 33.4 | 126.6 | 93.1 | 21.43 |

Figure 2 illustrates the percentage overlap between hours exceeding these thresholds and hours classified as heatwave periods by each detection method, disaggregated by room and performance indicator.

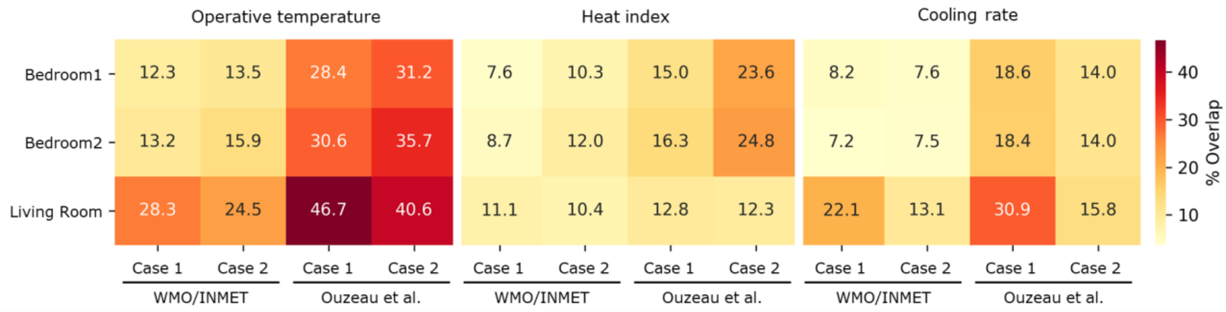


**Figure 3: Percentage of overlap between indoor indicators and detected heatwaves (Case 1 = high thermal inertia, Case 2 = low thermal inertia).**

Starting with operative temperature, the Ouzeau et al. (2016) method demonstrated a higher alignment with indoor thermal extremes across all rooms. The highest overlap was observed in the living room, while the bedrooms showed lower agreement. Since bedrooms are considered occupied in the simulation only during nighttime hours (22:00–08:00), the lower alignment with methods based on daily mean or maximum temperature is expected. Nevertheless, elevated nighttime temperatures can critically affect human health and should not be overlooked.

When using the Heat Index indicator, which combines air temperature and relative humidity, the alignment with detected heatwaves was lower in magnitude but revealed a distinct spatial pattern. The bedrooms exhibited a stronger synchronization with outdoor events than the living room, particularly under the Ouzeau et al. (2016) definition. This suggests that the periods identified as heatwaves by the detection methods did not fully capture the most intense overheating in the living room, where high dry-bulb temperatures were often accompanied by lower humidity levels, resulting in moderate thermal stress according to the Heat Index. The bedrooms, in contrast, showed a closer correspondence due to the higher humidity typically observed during nighttime hours, even under milder air temperatures. It is worth noting that humidity significantly influences the Heat Index only when air temperatures exceed approximately 26.7 °C.

The overlap between heatwave periods and extreme cooling loads was very limited for both detection methods. This indicator accounts for total (sensible and latent) loads, implicitly including the influence of humidity and solar radiation. As neither heatwave definition explicitly considers these variables, this result highlights a limitation in capturing periods of high cooling energy demand and potential stress on the electric grid. As with operative temperature, the living room exhibited a higher degree of overlap compared to the bedrooms.

Interestingly, while the Ouzeau et al. (2016) method exhibited a higher synchronization between Heat Index extremes and outdoor heatwaves in the lightweight insulated dwelling (Case 2), it aligned more closely with cooling load extremes in the heavyweight concrete case (Case 1). This opposite behavior may be related to the different physical nature of the two indicators and to how thermal inertia modulates the indoor response to outdoor heat stress. The Heat Index captures instantaneous conditions and therefore tends to react more directly to external temperature and humidity variations, particularly in low-inertia buildings. In contrast, thermal loads represent the integrated energy required to remove stored heat, which may increase during or shortly after prolonged heatwave periods in high-inertia envelopes.

## 4. Discussion

The results reveal that conventional heatwave detection methods, particularly those based solely on temperature thresholds, are limited in their ability to represent indoor thermal stress. Although both approaches were originally designed for outdoor climatological monitoring, their application to indoor contexts highlights important discrepancies.

The method proposed by Ouzeau et al. (2016), based on daily mean temperature percentiles, demonstrated greater sensitivity in identifying heatwave events throughout the historical series and better alignment with operative temperature extremes. This suggests that percentile-based approaches may be more suitable for studies aiming to couple outdoor and indoor heat-stress assessments. The differences observed between the bedrooms and the living room highlight the role of occupancy patterns and internal heat gains in shaping thermal stress, suggesting that exposure assessments based solely on outdoor thresholds may misrepresent actual discomfort risks.

When the Heat Index was considered, it revealed distinct spatial and temporal patterns. The bedrooms showed greater synchronization with outdoor events than the living room, especially under the Ouzeau et al. definition. These results emphasize that humidity can substantially influence thermal stress, even when temperature-based metrics indicate moderate conditions.

From an energy perspective, the weak correspondence between heatwave detections and cooling-load extremes indicates that the considered definitions fail to capture periods of maximum grid stress. This has implications for the design of resilient energy systems, particularly off-grid microgrids or battery-supported systems in tropical regions, where humidity and latent loads play a decisive role. Incorporating composite indicators such as the Heat Index or the Wet-Bulb Globe Temperature (WBGT) into heatwave detection frameworks may improve their relevance for energy resilience and thermal comfort assessments.

Although humidity was not explicitly included in the detection metrics, its influence was indirectly reflected in both the Heat Index and the latent component of the total cooling demand. Future research should test combined temperature–humidity thresholds and evaluate their temporal alignment with cooling rate peaks under different building typologies and occupancy schedules.

Beyond the building scale, identifying extreme events based solely on temperature may also limit the assessment of energy systems' resilience. Generation technologies such as photovoltaic and wind power are influenced by the combined variability of multiple climatic parameters, including solar irradiance, wind speed, and humidity.

This perspective aligns with recent discussions on compound extreme events, in which simultaneous anomalies in temperature, humidity, and solar radiation can jointly affect both energy supply and demand. Incorporating this multidimensional view would strengthen the connection between climatological metrics and the operational resilience of renewable-based systems. Extending heatwave detection frameworks to encompass multi-variable indicators could therefore enable a more integrated understanding of simultaneous stress on both demand and generation sides of the energy system.

## 5. Conclusions

This study assessed the correspondence between outdoor heatwave detections and indoor thermal and energy performance indicators. The main findings and implications are summarized as follows:

- Limitations of current detection approaches: Traditional methods, originally designed for outdoor monitoring, showed limited ability to represent indoor thermal stress and cooling demand.
- Operative temperature behavior: Moderate alignment with detected heatwaves was observed, with lower overlap in bedrooms (typically occupied at night, when physiological recovery is most critical).
- Heat Index analysis: By incorporating both temperature and humidity, the Heat Index offered additional insight into thermal stress behavior, with the higher overlap occurring in bedrooms.
- Cooling loads and energy implications: The mismatch was more pronounced for cooling loads, indicating that neither detection method adequately captures peak cooling requirements. This has implications for energy planning and system sizing, particularly for isolated or battery-supported microgrids under heatwave conditions. Including humidity in detection criteria may enhance correspondence with cooling needs due to its influence on latent loads and perceived discomfort, though this remains to be tested through further modeling and empirical analysis.
- Integration with renewable systems: Understanding the temporal overlap between indoor thermal stress and heatwave periods is essential for designing resilient solar-based cooling strategies. Combining photovoltaic generation, energy/thermal storage, and high-performance envelope retrofits can reduce grid stress and enhance passive survivability during compound extreme events.

Despite these insights, some limitations must be acknowledged. The analysis considered a single building typology without varying orientation, internal gains or occupancy profiles, which may limit generalization. Although this study already expands beyond operative temperature by including the Heat Index, both indicators still represent simplified proxies of human thermal stress. Future work should explore more comprehensive physiological models and extend the detection framework beyond temperature-based indicators to encompass the combined influence of solar irradiance, humidity, and wind speed. Such multi-variable detection approaches would enhance the understanding of simultaneous stress on both energy demand and renewable generation, supporting integrated planning for resilient power systems. Finally, as all results are derived from simulated data, field validation is recommended to confirm these findings and support design and policy decisions.

## 6. Acknowledgments

This work has been supported by the following Brazilian research agencies: CAPES and CNPq. The authors would also like to thank Saint-Gobain Re-search Brasil for the financial resources applied to this research development.

## 7. References

ABNT, 2024. Edificações habitacionais — Desempenho Parte 1: Requisitos Gerais (NBR 15575-1)

Bracht, M. K., 2025. Synchronization Analysis Code: Outdoor Heatwaves and Indoor Thermal Extremes. GitHub repository. URL: https://github.com/matheusbracht/swc_heatwave_synchronization/tree/main, accessed: October 2025.

Bracht, M. K., De Souza, L. P., Da Costa, V. A. P, Melo, A. P., Lamberts, R., 2023. Building simulation analysis using a 60-year historical weather series in Brasília/Brazil: How has the changing climate impacted the thermal performance of social housing? *Proceedings of Building Simulation 2023: 18th Conference of IBPSA,* Shanghai, 4-6 September. https://doi.org/10.26868/25222708.2023.1232.

Chen, X. Li, N.. Liu, J., Zhang, Z., Liu, Y. 2019. Global Heat Wave Hazard Considering Humidity Effects during the 21st Century. Int. J. Environ. Res. Public Health. 16(9), 1513. https://doi.org/10.3390/ijerph16091513.

Crawley, D; Lawrie, L., 2025. Climate.onebuilding.org. URL: http://climate.onebuilding.org, accessed: May 2025.

DOE, 2025. Auxiliary Programs – Weather Converter Program. URL: https://energyplus.readthedocs.io/en/stable/auxiliary-programs/auxiliary-programs.html#weather-converter-program, accessed: October 2025.

Faurie, C., Varghese, B. M., Liu, J., Bi, P., 2022. Association between high temperature and heatwaves with heat-related illnesses: A systematic review and meta-analysis. Science of The Total Environment. 852, 158332. https://doi.org/10.1016/j.scitotenv.2022.158332.

Gautier, A., Wetter, M., Sulzer, M., 2022. Resilient cooling through geothermal district energy system. Applied Energy. 325, 119880. https://doi.org/10.1016/j.apenergy.2022.119880.

Graczyk, D., Pińskwar, I., Choryński, A., Stasik, R., 2024. Less power when more is needed. Climate-related current and possible future problems of the wind energy sector in Poland. Renewable Energy. 232, 121093. https://doi.org/10.1016/j.renene.2024.121093.

Guo, S., Yan, D., Hong, T., Xiao, C., Cui, Y., 2019. A novel approach for selecting typical hot-year (THY) weather data. Applied Energy. 242, 1634–1648. https://doi.org/10.1016/j.apenergy.2019.03.065.

IEA, 2025. IEA EBC Annex 80 - Resilient Cooling of Buildings. URL: https://annex80.iea-ebc.org/, accessed: May 2025.

INMET, 2025. INMET Glossary - Heat wave. URL: https://portal.inmet.gov.br/glossario/glossario#O, accessed October 2025.

IPCC, 2023: Summary for Policymakers. In: Climate Change 2023: Synthesis Report. Contribution of Working Groups I, II and III to the Sixth Assessment Report of the Intergovernmental Panel on Climate Change [Core Writing Team, H. Lee and J. Romero (eds.)]. 1-34. https://doi.org/10.59327/IPCC/AR6-9789291691647.001.

Machard, A., Inard, C., Alessandrini, J.-M., Pelé, C. Ribéron, J., 2020. A Methodology for Assembling Future Weather Files Including Heatwaves for Building Thermal Simulations from the European Coordinated Regional Downscaling Experiment (EURO-CORDEX) Climate Data. Energies, 13(13). https://doi.org/3424 10.3390/en13133424.

Ouzeau, G., Soubeyroux, J.-M., Schneider, M., Vautard, R., Planton, S., 2016. Heat waves analysis over France in present and future climate: Application of a new method on the EURO-CORDEX ensemble. Climate Services. 4, 1-12. https://doi.org/10.1016/j.cliser.2016.09.002.

Perkins, S. E., Alexander, L. V., 2013. On the measurement of heat waves. Journal of Climate. 26(13), 4500–4517. https://doi.org/10.1175/JCLI-D-12-00383.1.

Roetzel, A., Tsangrassoulis, A., Dietrich, U., Busching, S., 2010. On the influence of building design, occupants and heat waves on comfort and greenhouse gas emissions in naturally ventilated offices. A study based on the EN 15251 adaptive thermal comfort model in Athens, Greece. Building Simulation. 3(2), 87–103, https://doi.org/10.1007/s12273-010-0002-7.